A Neural Network-based Low-cost Soft Sensor for Touch Recognition and Deformation Capture

Yifan Fan
University of Technology Sydney
Sydney, New South Wales, Australia
Yifan.Fan@student.uts.edu.au

Nico Pietroni
University of Technology Sydney
Sydney, New South Wales, Australia
Nico.Pietroni@uts.edu.au

Sam Ferguson
University of Technology Sydney
Sydney, New South Wales, Australia
Samuel.Ferguson@uts.edu.au

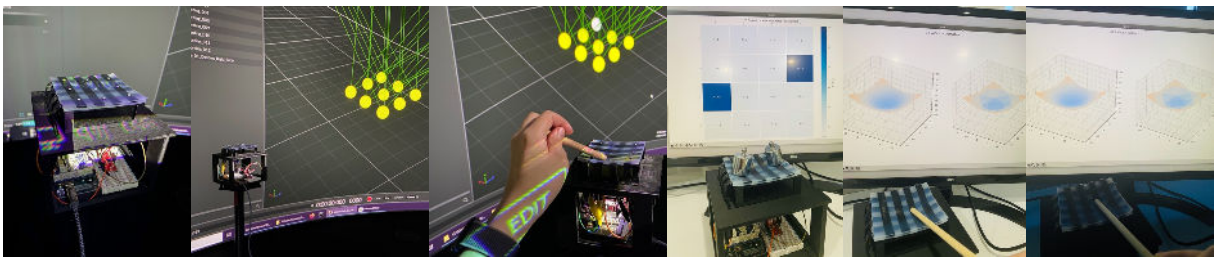

Figure 1: Our low-cost soft sensor detects contact areas, measures force, and reconstructs 3D virtual sensor surfaces in real-time. It identifies both single and multiple contact points and can reflect surface deformation in a dark environment.

ABSTRACT

We propose a novel, cost-effective soft sensor capable of detecting contact force, multiple touch points, and reflecting sensor interaction in real-time with a 3D virtual surface representation. Our fabrication process has been optimized for cost efficiency through careful material selection, utilization of automated machinery, and low-cost hardware. The sensor can be easily replicated without the need for complex laboratory equipment. The sensor employs trained neural network models for real-time signal translation into localization, force measurement, and deformation mapping. We have also developed an efficient data collection system that captures accurate 2D localization, force measurement, and 3D surface data to generate a high-quality pre-validated data set. This data set is filtered using prior knowledge before being fed to two neural network models. Our interactive prototype demonstrates the stability and accuracy of the low-cost soft sensor, delivering reliable results in both single-point and multi-point contact scenarios.

CCS CONCEPTS

• **Hardware → Sensors and actuators**.

KEYWORDS

soft sensor, capacitive sensor, deformation capture

DIS '23, July 10–14, 2023, Pittsburgh, PA, USA

ACM ISBN 978-1-4503-9893-0/23/07…$15.00
https://doi.org/10.1145/3563657.3595963

ACM Reference Format:
Yifan Fan, Nico Pietroni, and Sam Ferguson. 2023. A Neural Network-based Low-cost Soft Sensor for Touch Recognition and Deformation Capture. In *Designing Interactive Systems Conference (DIS '23), July 10–14, 2023, Pittsburgh, PA, USA.* ACM, New York, NY, USA, 15 pages. https://doi.org/10.1145/3563657.3595963

1 INTRODUCTION

For humans and other animals, the skin is one of the most fundamental means of perceiving the environment. No matter if we are shaking hands, touching an object, or being bitten by a fly, our skin allows us to feel contact forces and locate areas of contact. The term, wearable technology, has fueled a boom in wearable devices over the past few years, and soft sensors, which resemble biological skin, have become a hot topic in human-computer interaction. Flexible and stretchable sensors are naturally useful in the fields of robotic arms and interactive systems. However, assembling a soft sensor has proven to be challenging and costly. It's mainly due to the fact that the material used for the stretchable sensor is expensive and the fabrication workflow of embedded electrodes typically requires an industrial laboratory.

In an effort to overcome the challenges posed by the fabrication of soft sensors and maintain their performance, extensive research has been carried out. iSoft [65] and MultiSoft [66] have proposed the use of a toaster oven to form a conductive layer of carbon nanotube (CNT). However, this method is subject to reproducibility issues due to temperature variations and can only produce single-layer sensors. Another approach that aims to simplify the fabrication process involves the use of stretchable sensor arrays [12], but it requires the use of toxic solvents and poses environmental risks, making it difficult to reproduce in conventional laboratory settings. In our experience, the reproducibility of soft sensors is impacted not only by the material and temperature but also by factors such as the mold material, the amount of solvents used, and the mixing process. These variables can affect the sensor prototype, resulting

in a slowdown of interactive system research. Thus, it is imperative to develop a fabrication method that can be easily reproduced and achieve consistent results.

As illustrated in Figure 1, we present a novel, low-cost soft sensor that can be fabricated in a conventional university laboratory. To minimize costs and enhance stability, we have developed a fabrication workflow that leverages the capabilities of a 3D printer and laser cutter to minimize manual intervention and simplify electrode fabrication. Importantly, this process is executed without the use of any toxic solvents. The sensor is comprised of a shaped carbon nanotube (CNT) sheet and RTV (room-temperature-vulcanizing) silicone, resulting in a low cost of materials. The fabrication process is flexible, allowing for the production of sensors without strict device specifications. A challenge in the design of soft sensors is the connecting hardware, which can significantly increase the overall cost of the device. To address this issue, we have implemented an Arduino-based data reader, which simplifies hardware design and enables millisecond-accurate readings.

In this study, we adopt a data-driven approach to assess the precision of the sensor prototype. A real-time data collection system is implemented to gather ground-truth data, with a defined output format that encompasses both the force value and 2D position. To capture surface deformation, small reflective markers are attached to the surface of the soft sensors and their position is recorded in real-time using motion capture (MoCap) technology.

Following data collection, the raw data is subjected to several preprocessing steps, including data cleaning, moving averaging, and coordinate system transformation, based on prior knowledge of the geometric position. The processed data is then used to train deep learning networks to evaluate the accuracy of 2D localization under different testing scenarios. In addition, the accuracy of 3D surface deformation capture is evaluated using a test data set. Given its simplified fabrication method and cost-effectiveness, the interactive prototype holds significant potential for use in wearable devices and other interactive systems.

2 RELATED WORKS

Our work involves a wide range of fields, including deformable input and capacitive sensors. In this section, we briefly review the related works in these fields.

2.1 Deformable input

The research on sensor-based deformation capture and touch recognition have its roots in deformable input [1] [6]. Deformable input devices have primarily been utilized to replace traditional input devices regarding medical devices, controllers and smart mobile devices. Compared to the standard input devices such as the mouse and keyboard, the deformable input device offers a greater variety of shapes and sensing approaches [3]. For instance, the deformable input allows users to control the laptop through an interactive display. Wearable devices can be adapted to assist individuals with disabilities in their day-to-day activities. The fabrication principles of sensors are also diverse. Researchers have explored this domain using various flexible sensors. The majority of deformable inputs are designed to deal with specific obstacles. Thus, researchers tend to limit the capabilities of these sensors. For instance, [53] designed a sensor that can only identify stretching and has minimal use cases. The sensor described in [63] is only utilized to identify concrete cracks.

Research on deformable input devices can be divided into two categories: hand input and body input [39]. Due to the flexibility of human hands, deformable hand input is the focus of most research. Hand input deformation classes include bending, folding, stretching, and pressing, according to [32]. Bending is a common shape change, which often results in displays, handheld controllers [51], and musical instruments [34]. Folding often occurs in mobile phones, monitors, and some specific controllers. Typically, stretching is used in two-handed operations and one-handed stretchable sensors, such as pulling straps. The primary research context for deforming planes, touching screens and pressing sensors is pressing [5] [20] [54] [55].

Early research focused primarily on detecting a single type of deformation, known as one-dimensional deformation. In recent years, scientists have shifted their attention to multidimensional deformation, such as soft body inputs. Body inputs or wearable devices enable researchers to record the deformation of specific body parts using self-sensing devices [23]. For instance, Baldwin et al. [4] identifies the user's gait pattern and predicts whether or not they will fall. Singh et al. [50] categorises body positions. The reference [36] describes a recently developed pressure perception device. Parzer et al. [37] implements a sleeve to differentiate postures from raw data. Huang et al. [19] presents a sensor attached to the elbow that detects elbow movement. The sensor made by Ma et al. [27] can detect leg movement. By detecting the body's electric field with an integrated sensor, Yildirim et al. [64] augments the human body's sensing capabilities. The previous studies have contributed to the development of sensors with diverse shapes, forms, and applications. However, the requirement for specialized usage has posed a challenge in reducing the fabrication costs of these sensors.

2.2 Capacitive sensors

Capacitive sensors are associated with the research of human-computer interaction [16]. There are several fundamental characteristics of the capacitive sensor that have caught the attention of researchers. Capacitance sensing, for instance, utilizes only electricity, and the capacitor principle is simple [28]. A capacitive sensor consumes little power and its components are widely accessible and reasonably priced [18] [62]. Prior research has primarily focused on lowering fabrication costs, boosting sensor sensitivity for deformation, and implementing flexible sensors.

Since 1997, capacitance and electrodes have been integrated into touch sensors [23]. Murakami and Nakajima [31] introduced capacitive sensors as the hardware component of deformable input devices in the year 2000. By collecting the capacitance change with the input device, researchers can map the shape change to the capacitance change in the real world. The Sony research team implemented a deformable display utilizing a grid capacitive sensor in 2002 [40]. Changes in capacitance display can identify the location of finger contact. Through this research, occlusion defects caused by vision devices can be avoided. In 2007, researchers proposed a flexible, printed sensor [57]. Because the electrode distribution

has been pre-designed, the printed sensor can detect surface deformation. However, it is unable to pinpoint the location of the deformation.

To identify the location of touch and deformation, the researchers developed a microcontroller-based capacitive touch sensor [7]. This sensor is able to detect the precise location of the touch thanks to its 2D mesh structure. However, the sensor area is small and the sensing space is fixed. To bypass the shape restriction, Savage et al. [47] defined a method that can automatically cut the electrode layout based on the design. Copper foil is used to construct the sensor electrode, and a laser cutter is used to automate the cutting process. Such an approach overcomes the limitations of sensor shapes, allowing researchers to modify sizes and layouts to suit their requirements. Nonetheless, the sensor is not stretchable or foldable, and the copper wire is not durable. Consequently, Grosse-Puppendahl et al. [15] implemented a brand-new motherboard platform to reduce costs and improve robustness, linking up to 8 low-cost sensors.

To open up a path towards a large electrode number, Rus et al. [45] brought up the idea of 2D mesh structures for the electrode layout. Later, Gong et al. [14] reintroduced the printed electrode pattern to increase electrodes. Rendl et al. [41] described another printable electrode layout and sensor structure that significantly expands the number of electrodes and their coverage area. Utilizing the concept of Rendl et al. [41], Rendl et al. [42] proposed a redesigned sensor layout to sense folding. Later, Nguyen et al. [33] achieved a low-cost, flexible interface with new materials. This sensor is composed of conductive foam and fabric and can locate the spot of the deformation on the 3D model. It requires 8 nodes to capture the direction of folding but fails to reflect the deformation's details.

From a different angle, Mehmann et al. [29] implemented a flexible input with 56 electrodes and attempted to capture the shape of the bump layout. In 2015, Schmitz et al. [48] embedded conductive carbon-based materials into 3D-printed models. The shape of the conductive materials can be flexible. In the same year, Weigel et al. [59] designed a novel type of flexible sensor that allows users to design the shape and size of the sensor with laser cutting. The capacitive circuit is composed of cPDMS (carbon doped polydimethylsiloxane), and the laser cutter can also be used to shape the layout of cPDMS. Although the sensor can only detect the pressing and not the location of the contact, its design has inspired future research such as [22]. After that, a new elastic and flexible electrode material was developed [2]. In this work, the fabrication complexity of capacitive sensors was reduced by automating the workflow. Casting materials, laser-patterning electrodes, and applying a protective layer consists of the standard fabrication process. PVA (Polyvinyl alcohol) is used to adhere the circuit to the surface of PDMS (Polydimethylsiloxane), which simplifies the production workflow. The fabrication process has been further developed by subsequent studies conducted by Glauser et al. [12] [13] and Yoon et al. [65] [66]. These studies have demonstrated that soft sensors based on a combination of carbon and silicone materials can be produced at a low cost while still retaining their sensitivity.

2.3 Fabrication

Initial research directions for fabrication are concentrated on material breakthroughs. Sensor performance is typically improved by increasing the conductivity and flexibility of the materials. As a result of the invention of novel materials, the workflow for fabricating objects becomes heavily complicated, and the price tends to increase vastly. For instance, Sekitani et al. [49] provided SWNT-based (Single-Wall Carbon Nanotubes) stretchable conductors. Thus, the fabrication process requires a high-pressure jet-milling homogenizer and the continuous addition of various materials to the gel. It has restrictive temperature and time requirements.

To reduce the complexity, researchers proposed various solutions with cheap materials. Grosse-Puppendahl et al. [15] described the motherboard and the sensor link. Wikström et al. [61] utilized the conductive tape to perform sensing. Grosse-Puppendahl et al. [16] introduced wires and sheets to construct the sensor. Although these sensors reduced costs, the sensor materials are not standardized, and each solution has a unique fabrication process. And therefore, the production process necessarily requires a fair bit of manual work, resulting in a massive influence on sensor precision.

Over the years, scientists have invented automated fabrication using cutting machines and automatic printing mechanisms. Through the use of cutting machines, Savage et al. [47] achieved flexible copper circuits. Gong et al. [14] designed an automated manufacturing process that prints the layout of copper electrodes. Kao et al. [22] produced the circuit layout by slicing the gold leaf. Peng et al. [38] designed and implemented a new type of 3D printer, which is capable of printing deformable and complex objects directly. Besides this, it can also print multilayer circuits. The printed model, however, is relatively rough. Araromi et al. [2] described a flexible and stretchable single-layer electrode circuit material, and most of the processes were automated. This stretchable material's substrate is composed of PDMS. PVA plane is formed by casting, and during fabrication, unshaped electrode layers are covered with screening on the PVA plane. The circuit is then printed via laser patterning. Wessely et al. [60] used UV lithography to print the sensing area. Rosset et al. [43] presented a fabrication approach in which the stretchable film was attached to the placeholder and printed by machines. By 3D printing a sensor mold and squeegeeing conductive ink, Jeong and Lim [21] minimized the amount of manual work.

In addition, screen printing can also be achieved through shadow masks [49]. Later, Cholleti et al. [8] described a novel method for simultaneously printing conductive ink and conductor material. Yoon et al. [65] mixed the nano-titanium tube material with other substances to make a flat surface. During the manufacturing process, they utilized a heat press and toast oven to accelerate the curing. Unlike the previous production process, this fabrication workflow can be re-implemented in the laboratory setting. Yoon et al. [66] also strived to use the toast oven in the production process. However, the electrodes of the above-mentioned sensor types only consist of a single layer. Moreover, researchers have integrated laser cutters into fabrication steps in an attempt to streamline production [27] and inspired our work.

2.4 Analysis approach

The analysis approach of capacitive sensors is closely related to the sensor layout. The simplest electrode layout involves positioning the sensor at a predetermined location and capturing touch or deformation via sensor data changes at each predetermined location. The approach described by Grosse-Puppendahl et al. [15] involves the placement of up to eight touch sensors in a predetermined scene. Lissermann et al. [26] developed a wearable ear device that can respond to both single and possible multiple touches. The device can be used as a controller for playing music, adjusting the volume, and pausing the music by touching the predefined sensing area. Wikström et al. [61] provided conductive tape with motionless electrodes. Thus, only a few deformations can be gathered. Additionally, the wearable sensor provided by Singh et al. [50] has fixed electrode positions. Parzer et al. [36] used rows electrode to measure pressure. Sarwar et al. [46] proposed the grid sensor array to identify the location of the touch. Han et al. [17] designed a deformable flexible plane with linear hall sensors and permanent magnets that can reflect the touch on the plane of a virtual environment in real-time. Through marker detection and camera-based prior knowledge, Rendl et al. [42] achieved the real-time correspondence between the 3D plane and the sensor plane in [33] constructed a virtual 3D model that includes eight pre-installed nodes.

Algorithms and techniques for machine learning and deep learning open up a path to map raw data to corresponding deformations. Cohn et al. [9], for instance, employs KNN (k-nearest neighbors) to map the raw data collected by wearable devices across multiple body actions. Yoon et al. [65] analyzed the deformation and movement collected by the Neighboring Method through linear regression. As a classic algorithm of machine learning, SVM (support vector machine) is also used. Cohn et al. [10] utilized SVM to map electronic noise to various pose classifications. Nguyen et al. [33] identified the direction of the deformation correctly by SVM. Parzer et al. [37] designed a sleeve sensor to collect posture-related deformation and determine the correct posture through SVM. SVM also works well with NeighboringMethod [66].

The problem of identifying the touch position was also viewed as a regression problem by researchers [25]. Thus, they adopted the random decision tree forest to process the regression calculation. Rus et al. [44] opted to use a decision tree to analyze the original data and obtained positive results. After that, Vega et al. [58] identified the subconscious movement through the decision tree. Singh et al. [50] implemented a wearable device to recognize body posture with decision trees. Mohd Noor et al. [30] utilized PCA to reduce the dimensionality of the original data and introduced the Gaussian Process Regression model to predict finger movement. In recent years, Larson et al. [24] built a grid-like electrode distribution sensor and analyzed the raw data through CNN (convolutional neural network) to identify the touch position in real-time. FCN is additionally mentioned in [12] and [13] and perform positive results.

Inspired by previous research, we aim to explore the potential relationship between sensor data and surface deformation using deep learning networks. Our experimentation has revealed that fully convolutional networks (FCNs) and convolutional neural networks (CNNs) can effectively enhance the performance of grid-mesh soft sensors, with performance being dependent on the size of the grid mesh.

3 SENSOR DESIGN AND FABRICATION

The objective of this study is to design a flexible and economical sensor that can be assembled in a university laboratory setting while providing an acceptable level of accuracy. We aim to reduce the cost of our sensor through several strategies, including the optimization of material selection, electrode design, sensor hardware, and fabrication workflow.

3.1 Conductive Material

The current research trend in soft sensors is largely focused on industrial-grade sensing systems, which are challenging to replicate and require sophisticated production environments, leading to significant cost implications. However, even flexible sensors that can be assembled in a laboratory setting are subject to limitations in terms of replication success, which is often dependent on the availability of proper equipment. For example, the mixing of carbon nanotube material with liquid silicone to achieve uniform conductivity requires a high-powered stirrer. The curing process of silicone also presents challenges, as high temperatures are required to solidify the material, and any air bubbles present may expand and negatively impact surface flatness. Additionally, the mixing of conductive carbon and silicone necessitates the use of toxic solvents such as Toulon and isopropyl alcohol, which emit harmful volatile gases during the curing process.

To simplify the fabrication process and reduce costs, we carefully selected the conductive material. We considered conductive fabric and ink, carbon powders, and CNT materials but found that they either lacked stretchability or required a complex fabrication process. Conductive fabrics have been extensively utilized in prior studies. However, the production of conductive fabrics is comparatively more complicated than that of silicone-based sensors. Typically, it involves the weaving of conductive materials with fabrics, which necessitates the use of specialized equipment. Due to limited access to materials and fabrication equipment, replicating a fabric soft sensor may present a challenge for other researchers. Additionally, the stretchability of textiles is inferior to that of silicone materials. Eventually, we chose to use TUBALL MATRIX 601 CNT sheets [56] for their good stretchability and reasonable cost. The volume resistivity of the conductive sheet is $1.10\hat{2}$ Ω.cm. Each sheet is 0.14m x 0.14m, 2mm thick, weighs 0.045 kg and costs only 34 USD. Using half a sheet per sensor reduces the conductive material cost to 17 USD per sensor. The use of CNT sheets greatly simplifies the sensor fabrication process and minimizes complexity.

3.2 Multi-Layer Structure

The final prototype sensor is depicted in Figure 2. Our flexible sensors have a translucent appearance, with the distribution of electrodes and conducting circuits visible on the surface. The sensors have a five-layer structure consisting of two protective layers, a dielectric layer, and two conductive layers. The dielectric layer, composed of silicone RTV 4420 components [11], is made from the same material as the protective layers and can be cured at normal room temperature without the use of toxic solvents.

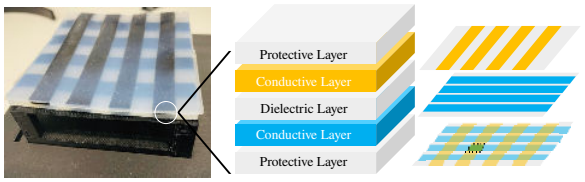

Figure 2: Left: A prototype soft sensor. Middle: A five-layer structure for the soft sensor. During deformation, the distance between two conductive layers changes, causing a variation in capacitance. Right: Circuits are embedded within each conductive layer. The parts that overlap function as electrodes for our soft sensor.

The low cost of the primary material used in the sensors is a key advantage, with each flexible sensor costing less than 20 USD (excluding the 3D-printed support frame and electronics) and having a total thickness of less than 4 millimeters. The sensors feature extensions on both sides to connect the circuits to the data reader. The current dimensions of the flexible sensors are 9 cm by 9 cm. The sensors can self-calibrate and begin outputting capacitance data in less than three seconds with a reading frequency measured in microseconds, eliminating the need for additional equipment in the setup process.

The two conductive layers of the flexible sensor have distinct circuit distributions that intersect in the vertical direction at the electrodes. The flexible sensor recognizes touch events through changes in the capacitance of these electrodes. The stretchable and deformable nature of the layers enables the sensor as a whole to be stretchable, deformable, and foldable. As a capacitive shape-changing sensor, the capacitance value of the sensor capacitor is not fixed and depends on the overlapping area and distance between the two electrodes. During deformation, the distance and overlap area between the electrodes change, and the real-time change in capacitance allows the sensor to determine the location and extent of the deformation.

The electrodes of the sensor are arranged in a grid pattern with 16 electrodes formed by the natural intersection of the conductive layer circuits. The grid layout simplifies data collection and visualization, as well as facilitating correspondence between the weight map and electrode positions. Reflective markers were used to collect 3D geographic data, and the grid layout of the markers can be matched to that of the electrodes for easier validation of the dataset.

3.3 Hardware

The data reader is primarily composed of an Arduino motherboard, a multiplexer, and a 3D-printed frame. Utilizing the Arduino motherboard as the prototype's hardware significantly reduces production costs. The data reader's primary function is to rapidly measure the current capacitance of each electrode. During capacitance measurements, the multiplexer is able to swiftly switch between circuit channels. As illustrated in the Figure 3, the data reader measures the current capacitance of the electrodes through the red channel S. When the red channel is connected, the Arduino board records the amount of time required for the capacitance of the electrodes to fill with the current voltage. The data reader's processing time can be

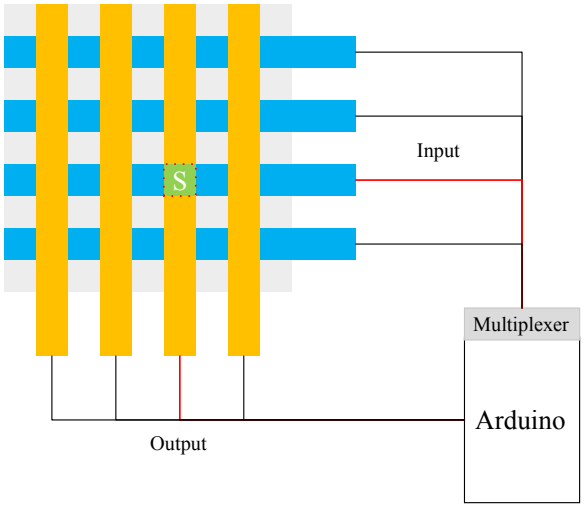

Figure 3: Capturing the capacitance value S of the sensor electrode that is activated. The data reader is composed of an Arduino board and a multiplexer. After activating the red circuit, the reader is able to collect the value S. By switching multiplexer channels, the capacitance of each electrode is obtained.

used to calculate the electrode's current capacitance. As soon as the output is completed, the multiplexer switches to the next channel. This procedure is repeated until the entire reading is complete. In the invariant state, the entire capacitance of the electrodes can be read in approximately 0.5 microseconds. In a state of deformation, the total time alters to around 0.9 microseconds. The script installed on the Arduino board keeps track of the current electrode coordinates, capacitance value, and timestamp automatically.

3.4 Fabrication process

The use of automated machines such as laser cutters and 3D printers is crucial in reducing sensor cost. Previous research has shown that these machines can decrease manual labor and create complex circuits, leading to cost reduction and improved reproducibility. The manufacturing process consists of two workflows, as shown in Figure 4. Firstly, a conductive layer with the designed electrode layout is produced using a laser cutter. The electrode layout is based on the capacitive principle and the CNT sheet is cut by the laser machine to have a predetermined electrode layout. The cut electrodes may stick to the base due to the high temperature of the laser cutter and must be cleaned with water and a towel before use.

In the second step, sensor molds are prepared using a 3D printer. PolyCarb is printed as the material on a Stratasys 450mc 3D printer [52] and both sides of the mold have extended circuit interfaces. The main component of silicone, RTV 4420, is mixed with component B to form a liquid silicone that contains many air bubbles after mixing. The next step is manual stirring for 15 minutes to produce a clear mixture without air bubbles. As shown in Figure 4, the protective layer is created by pouring the silicone mixture into the basement mold. This layer, made entirely of silicone, is the lowest layer of the soft sensor and has a thickness of 1 millimeter after natural

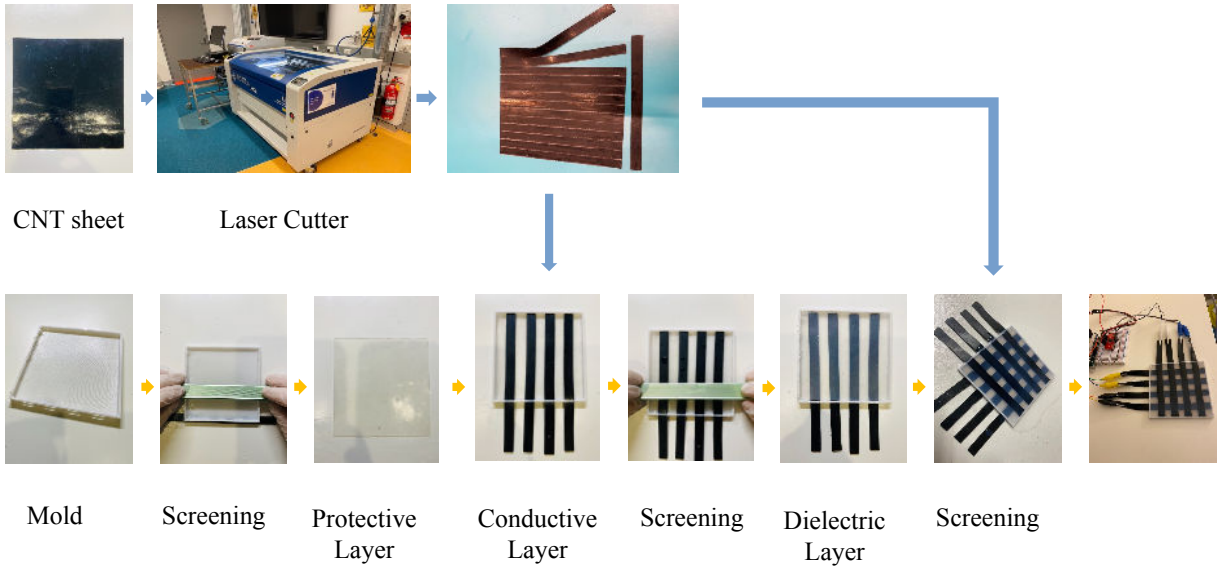

Figure 4: The fabrication of a soft sensor involves two pipelines: the upper one is for laser-cutting conductive layers and the lower one is for fabricating the multi-layer sensor.

curing. The extra silicone liquid is removed from the mold using a squeegee.

Next, the protective layer is placed within the mold for the dielectric layer and the previously generated electrode layout is positioned on top, with the electrode ends protruding from the mold. The mold is then refilled with the silicone mixture and any extra liquid is squeezed out. After natural cooling, the first conductive and dielectric layers are formed. This process is repeated to create the remaining layers, including the final protective layer, resulting in a fully functional flexible sensor with a thickness of 5 mm that is extensible and deformable.

After the sensor is formed, a data reader is used for quick verification by reading the capacitance data of each electrode. In this study, we have opted for a non-toxic manufacturing method by allowing the silicone to cure naturally, avoiding the use of harmful solvents. The curing process can be carried out at room temperature, taking approximately 6-7 hours per layer. The overall production time for a single sensor is approximately 2 days. Although this may seem like a considerable investment of time, it is a necessary cost to ensure the safe execution of the experiment within a standard laboratory environment.

4 DATA ACQUISITION

To verify the efficiency of our soft sensor, we utilize a data-driven approach. The success of this approach is dependent on the availability of a large and reliable dataset. Since our sensor solution is novel, no pre-existing dataset is available. Thus, we developed a custom data collection workflow from scratch. The workflow focuses on rapidly collecting high-quality data with minimal noise to ensure the accuracy of the deep learning model. The data collection process is divided into two stages: two-dimensional touch sampling and three-dimensional deformation sampling. The goal is to detect two-dimensional touch and accurately reconstruct the three-dimensional deformation of a plane.

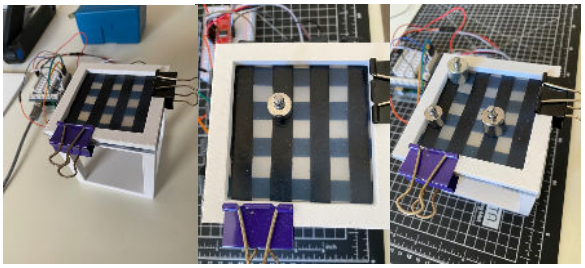

Figure 5: Left: Weight and force collector prototype. Middle: Collect touching localization and force. Right: Collect data of multiple touching

4.1 2D Touch Sampling

As depicted in Figure 5, we have established a supporting structure for 2D touch detection. The sensor is centrally positioned in the frame and attached to its edges. Contact position and force are determined using calibration weights. Different weight options are available to gather sensor raw data, and multiple copies of the same weight can be used to capture multiple touch data. A weight map has been created to standardize data input and output, displaying both touch position and force (see Figure 7). The weight map's grid is mapped onto the electrode pattern, and when the sensor surface is covered with weights, the corresponding weight map is represented numerically with units in g.

During data collection, calibration weights were placed on the soft sensor's surface and weight maps were adjusted accordingly. We developed a data collection script that integrates unprocessed

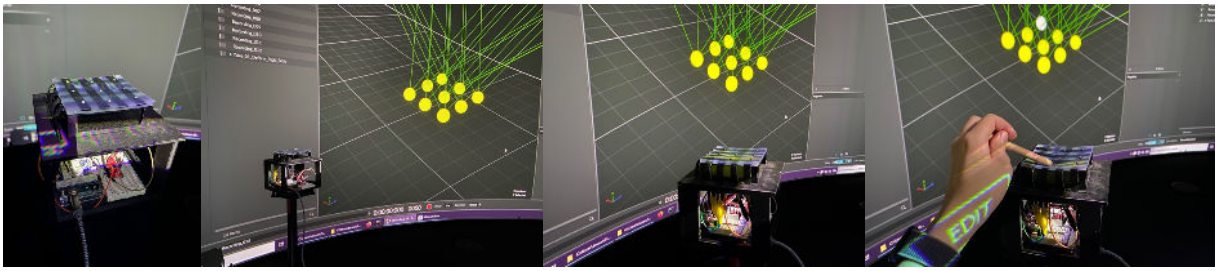

(a) (b) (c) (d)

Figure 6: (a): Reflective markers attached on the surface. (b): Data collector with OptiTrack system. (c): The initial state of marker's position. (d): Recording the deformation of our soft sensor.

data with the weight map in real-time, streamlining and accelerating the data collection process. The script verifies that the weight map corresponds to the weight's actual position, and can temporarily halt data collection if erroneous data is detected. The script also confirms storage location and checks for existing data before collection begins. After data collection, the script asks if another round should be initiated. To enhance data quality, we applied a moving average calculation, which computes the mean of 32 records per electrode. The script can store up to 100 records per scenario and format the raw data and weight map accordingly. The final dataset includes capacitance values, weighting plots, and moving average spans for each electrode. With the script, a single touch point with the same weight can be sampled in under 20 minutes, and we can currently sample over 30,000 records per cycle.

When conducting data collection, several important considerations must be taken into account. The initial value of the flexible sensor may vary slightly due to environmental factors, leading to some variations in the collected data. To address this, the initial data is collected from the sensor in its stable state and used for calibration during data processing. It is also important to note that the initial values of electrodes may vary slightly due to their physical state. To preserve positional data, it is crucial to ensure that the data collection sequence matches that of the electrodes.

4.2 3D Deformation Sampling

To generate a dataset for deformation data, we utilized vision-based solutions. With the advancements in deep learning networks, motion capture systems, such as OptiTrack [35], have become more advanced and have been adopted as industrial solutions by many leading research teams and businesses. OptiTrack's advantage is its ability to track the 3D positions of reflective markers in real-time. To collect information on the soft sensor's 3D deformation, 9 reflective markers were affixed to its surface with a size of 3mm and a grid layout was assigned to them. To read and record sensor data, a collection script was also developed.

The sampling was conducted in a laboratory equipped with 18 OptiTrack cameras, capable of capturing real-time 3D geographic data of 3mm markers. To enhance sampling precision, a black framework that minimizes light reflection was designed to hold the soft sensor, data reader, and be placed on a camera holder. The OptiTrack system records 120 frames per second and identifies unique markers during the sampling process. After sampling, the raw sensor data was merged with the 3D geographic data and timestamp to obtain a comprehensive dataset.

The motion capture system, as shown in Figure 6, labels the captured markers on a large display. To avoid losing the position information, it's essential to keep track of the marker status and change from yellow to white. The markers are sampled for 1 to 2 minutes to reduce the chance of loss, and the number of cameras used for tracking is limited to four to improve accuracy.

During the acquisition process, the data collection script logs the sensor's capacitance values, followed by the motion capture system tracking the markers' 3D positions in real-time. A wooden stick is used to touch the sensor surface and record the change in the marker's position, which is displayed in real-time. It's crucial to be cautious while collecting the data, as missing a marker due to its small size or encountering an obstruction may result in repeating the sampling process. The acquisition process lasts approximately 1.5 hours, and a single round of acquisition results in approximately 48k 3D position records.

4.3 Pre-validation

After data collection, it is essential to assess the quality of the collected data to ensure it meets the required standards. The performance of a data-driven model heavily relies on the accuracy of the data set used to train it. A well-curated, clean and valid data set makes it easier to identify and resolve model issues, leading to increased precision. However, data collected can sometimes be affected by external factors, resulting in biased or incorrect data. This can negatively impact the accuracy and validity of the model. To mitigate this risk, further validation is necessary to determine the suitability of the collected data for building a data set.

After collecting the 2D touch and 3D deformation data, it's important to verify their accuracy. This is because the performance of a data-driven model is dependent on the quality of the data it's trained on. To validate the data, a deep learning model is pre-trained and used to make predictions based on the sampled data. The pre-validation process involves feeding the data into the model and generating a weight map based on the input.

The focus during pre-validation is not on the accuracy of the predicted weight map, but rather on identifying any significant deviations from it. This is done by comparing the predicted weight

map with the actual data and visually inspecting the results. If there are significant positional errors or differences in value, the sampling procedure is re-evaluated to determine if an operational error has occurred. For 3D deformation sampling, a similar pre-validation process is used with a unique pre-trained model, FCN-P, which is specifically trained for 3D deformation capture. The visualization graph used to validate the predictions is a 3D geometric graph.

5 COMPUTATION APPROACH

5.1 Data Processing

Before using the data set to train the deep learning model, the data quality must be enhanced. The initial step is to standardize the raw sensor data. Since the capacitance value of the soft sensor varies during surface deformation, we want the learning process to emphasize value variation. Therefore, the sensor data must be normalized by comparing the initial state to the changing state. As a result of the sampling process, we can obtain the capacitance value during the initial state, which is then utilized to generate the normalized sensor data. During the second step, sensor data is located using an electrode grid. Due to the fabrication process, the initial state value of each electrode varies slightly. Both the weight map data set and the 3D geography data set must be converted to the same electrode order. Therefore, the positional information can be mapped.

For the 3D geographic data, additional processing steps are required. The first step of the process is to sort the 3D geography data. Multiple rounds of raw data collection were conducted by the OptiTrack system. For each sampling workflow, the OptiTrack system will assign reflective markers a random identifier. Therefore, we must reorganize the order of the 3D geography data makers. This was achieved by analyzing the 2D geographic data. During the deformation, the vertical direction has changed significantly relative to the horizontal plane. Using the marker's grid layout, we can quickly locate the position data. Converting Cartesian coordinates to Laplacian coordinates is another necessary step. Laplacian coordinates are widely used for surface deformation and three-dimensional mesh deformation. Laplacian coordinates, as opposed to cartesian coordinates, emphasize the relative relationship between closed pinpoints. By converting the unprocessed data set to laplacian coordinates, we can eliminate the impact of orientation and angles. To obtain laplacian coordinates, the neighboring points of each marker must be specified. Based on the visual representation of 3D geography data, we observed that the X-axis and Z-axis plane has a stable change, and we can use the relative position on the 2D plane to define neighbors. The entire data set's Laplacian coordinates were then generated utilizing the neighbors mapping.

All data processing operations are performed by developed scripts. For data processing, only the file paths and target paths of the files must be modified manually. Before using them for normalization, the script calculates the initial values of each sample. The only operation that requires human intervention is the arrangement of 3D coordinates. This step requires an inspection of the current data visualization.

Table 1: Comparison of weight map prediction using FCN-W and CNN-W(Convolutional Neural Network) network models. From left to right: two different network models. From top to bottom: the average weight loss of model trained on different scenarios. The FCN-W model shows improved performance in multi-touch scenarios compared to the CNN-W mode.

Model	FCN-W	CNN-W
Single-touch Error	3.96	5.03
Multi-touch Error	1.81	7.38

Table 2: Comparison of different network models for weight map prediction. From left to right: two different network model. From top to bottom: the normalized distance loss of model trained on different scenarios. FCN-P model achieves similar result with CNN-P model.

Model	FCN-P	CNN-P
Error	4e-5	2e-5

5.2 Model Architecture

Our model architecture aims to reflect the real-time surface change of our soft sensor. Two lightweights, fully connected neural networks (FCN) are used to construct this capability. Sensor electrode capacitances S are the input data set for both FCN models. During data processing, each input data $S \in \mathbb{R}^{16}$ is normalized and can be used for two FCN models simultaneously. For touching force and contact localization, we map each input data S to a weight map output $W \in \mathbb{R}^{16}$ using the FCN model (FCN-W). As described in the section on data collection, the weight map W contains the weight of the touching force and location. For the deformation tracking, we employ an additional FCN model (FCN-P) that maps sensor data input S to marker positions with laplacian coordinates $P \in \mathbb{R}^{3\times M}$. M is the number of markers, which is nine, and P represents the relative positions between markers.

Figure 7 and Figure 8 depict the network architecture of the FCN-W and FCN-P models. FCN-W and FCN-P both include a 16-unit input layer. The input layer is followed by three fully interconnected hidden layers in the FCN-W model. Each of the first two hidden layers contains 2048 units, while the third and final hidden layer has 1048 units. The final output layer includes 16 units that predict the weight map values. Following all hidden layers and the input layer is the ReLu activation function. FCN-P shares the same architecture as FCN-W with the exception of the output layer. 27 units reflect the predicted position P in the output layer of FCN-P.

We conducted experiments with a 2D-based network, the CNN (Convolutional Neural Network), to capture and reflect 2D information in the results. We compared two CNN models to FCN-W and FCN-P. Table 1 and table 2 show that the FCN-W and CNN-W models have comparable performance in single-touch scenarios. However, the CNN-W model performed poorly in multi-touch scenarios. In terms of 3D position prediction, both FCN-P and CNN-P had similar results. We observed that the CNN model required more

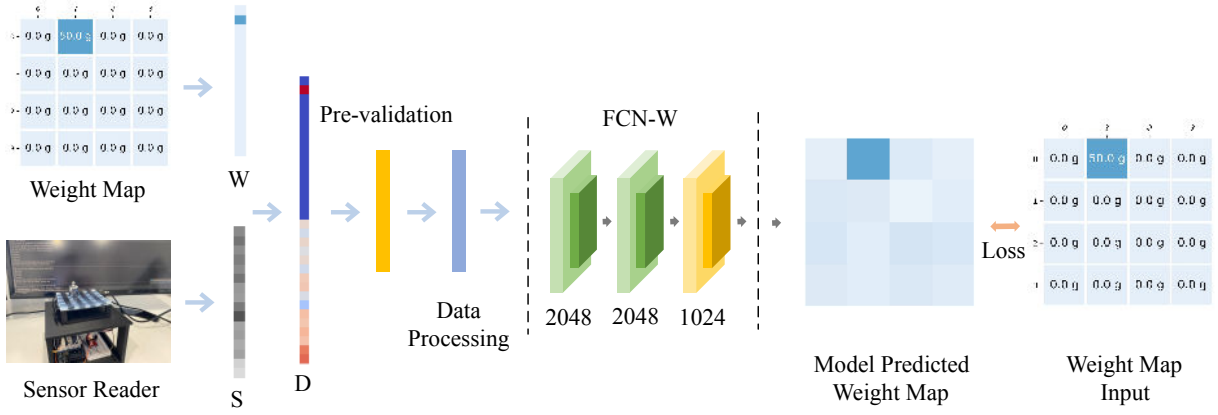

Figure 7: Left to right: the data collection and training process of the FCN-W (Fully Connected Network) model. W is the vectorized input for the weight map, and S is the vectorized input for the sensor capacitance. Before becoming the FCN-W model's input, the data set D will undergo pre-validation and data processing. We evaluate the model's performance by measuring the loss between the predicted output and the actual input.

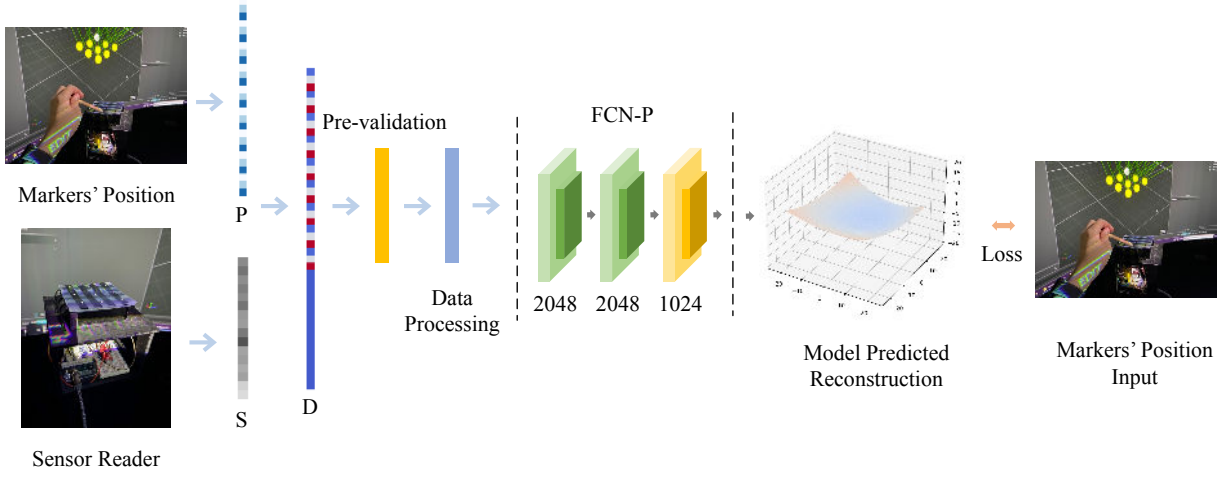

Figure 8: Left to right: the FCN-P model's data collection and training processes. P is the vectorized input for the 3D location of reflective marks, and S is the vectorized input for the sensor capacitance. D represents the merged data set records by timestamp. We enhance the performance of the model by decreasing the distance between the predicted marker locations and the actual input.

epochs and training time compared to the FCN model, and the 4x4 sensor resolution restricted the CNN model's output. It is difficult to upsampling the features with 4X4 resolution. As a result, we opted to use the FCN model for our final prototype.

The FCN-W and FCN-P models were implemented using PyTorch and trained with a squared L^2 loss. The ADAM optimizer with a learning rate of 10^{-3} and weight decay of 10^{-5} was utilized for both models, with a batch size of 64 during training. The FCN-W was trained for 20 epochs, while the FCN-P was trained for 4 epochs. The CNN models were also implemented using PyTorch, consisting of 2 Conv layers followed by 3 fully-connected layers. The loss function used was MSELoss and the optimizer was Adam, with a learning rate of 10^{-3} and weight decay of 10^{-5}.

6 TASK EVALUATION

To establish the efficacy of our soft sensor, we meticulously design and gather data sets from a range of scenarios. Our experiment employs a model that has been trained with data from each potential scenario. To evaluate the accuracy of each scenario, we designate one set of data for testing. As depicted in Figure 11, our experiment utilizes an integrated soft sensor and data reader, which has been 3D-printed. The sensor is seamlessly linked to a data reader based on the Arduino platform.

To operationalize the trained models, we have developed an application script that can retrieve sensor data in real-time and load the trained models dynamically. The script is capable of reconstructing out-of-sight deformations without relying on a vision-based

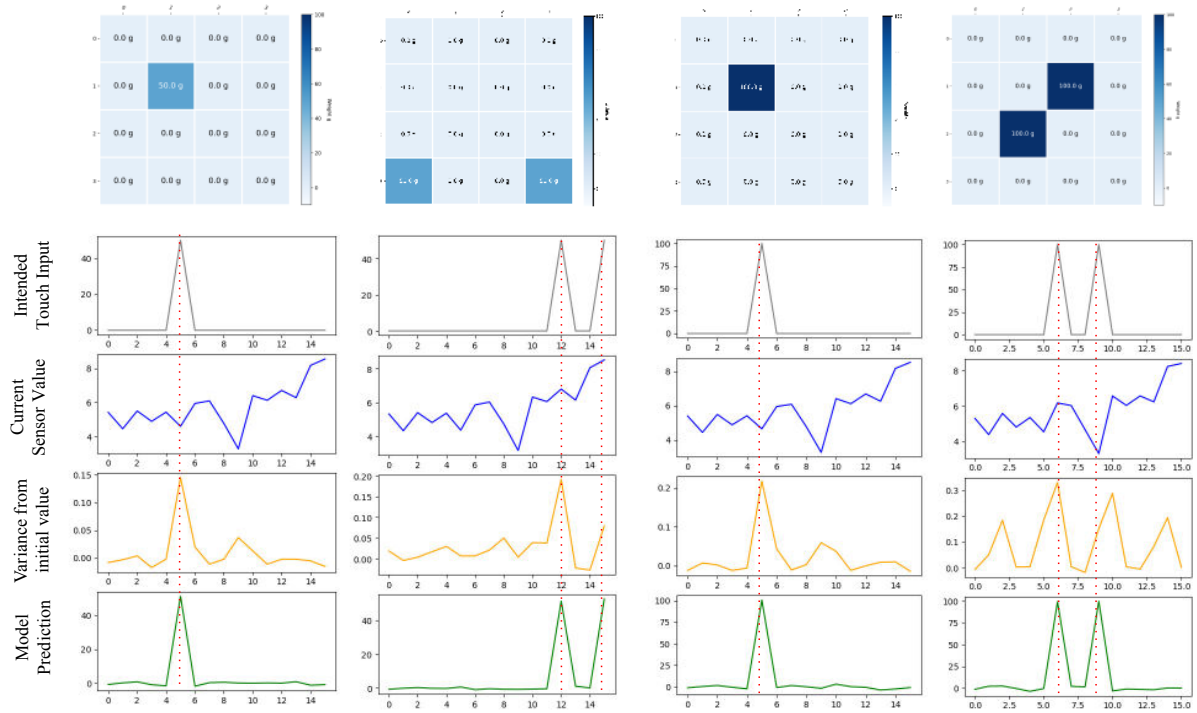

Figure 9: From left to right, there are four distinct weight maps: 50g single-touch, 50g multi-touch, 100g single-touch, and 100g multi-touch. From top to bottom are arranged the vectorized weight map, the capacitance value of the sensor, the change in capacitance value, and the predicted value after training. The dashed lines depict the quantitative relationship between touch position and sensor data.

solution. Once initiated, the script's data-reading function continuously collects raw sensor data at millisecond intervals. The raw data is then processed, sorted, and normalized into the appropriate input format, $S \in \mathbb{R}^{16}$. The regression function then loads the same input into the pre-trained FCN-W and FCN-P models. After the prediction process, we obtain the current weight map $W \in \mathbb{R}^{16}$ and the real-time 3D position of nine markers $P \in \mathbb{R}^{3\times9}$. The outcomes of W and P are represented visually as images.

6.1 Contact Localization and Force Detection

The prototype and data set are validated through two methods. Firstly, our data set includes test data that can be used to assess the training model's accuracy. Secondly, to test the model's generalizability, we perform experimental tests with the developed interactive system and calibration weights across various scenarios. As shown in Figure 9, the test scenarios encompass four distinct categories: 50 g single-touch, 50 g multi-touch, 100 g single-touch, and 100 g multi-touch. By utilizing the data collection script, we were able to gather information on these scenarios within a period of 30 minutes. To account for the large number of possible multi-touch combinations, we selected 22 patterns for the multi-touch weight map and collected information on these patterns. The entire data collection process took approximately 1 hour and 15 minutes, and the newly obtained data was used to train our models. The test data served as the benchmark for our prototype, which predicted the location of the touch with 100 percent accuracy. The trained model demonstrates proficiency in predicting both single and multi-touch events, along with the corresponding force weight measurement. With an average error of 2.29 g, the touch weight measurement predictions are highly accurate. The prediction results clearly indicate that as the touch force increases, the capacitance of the flexible sensor increases proportionally, as seen through visualizations.

To assess the model's generalization capability, we used calibrated weights and the prototype system. As depicted in Figure 11, the prototype system can accurately detect the position and weight of weights placed on the flexible sensor in real-time. To enhance the system's stability in the prototype, moving averaging was employed to filter the input data. 20 rounds of generalization tests were performed under these conditions, with the system successfully predicting 100 percent of the touch's 2D position information. The average touch force measurement error was 5.6 g, with a maximum error of 12.9 g and a minimum error of 0.2 g. It was found that increasing the moving averaging time to 3 seconds significantly reduced the maximum error. During the generalization test, we observed that the weight's position influenced the final weight value. The closer the position was to the electrodes, the smaller the error in the final weight value. To further improve the performance,

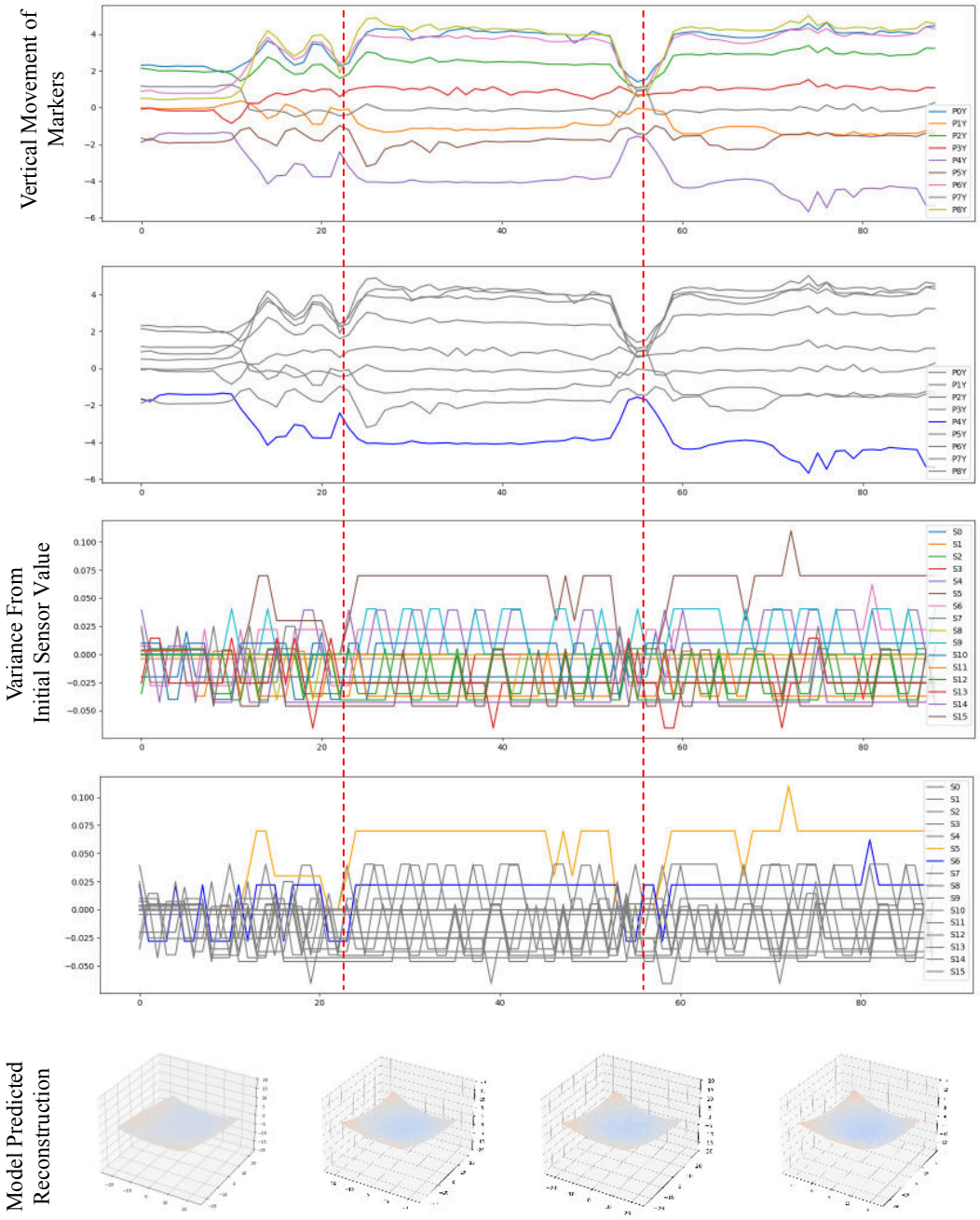

Figure 10: The two images at the top illustrate the change in vertical position of markers during deformation. The second graph highlights the vertical position route of the central marker. In the two middle plots, the the corresponding sensor capacitance variance values are represented. Changes in the electrodes adjacent to the central marker are highlighted. The 3D-reconstructed plane, predicted by our prototype system, is located at the base of the image. The dashed line displays the relationship between the vertical position of the marker and the capacitance variation.

we trained fine-tuned models for each test scenario, resulting in a reduction of the average error in the generalization test.

Figure 11: A gallery of use cases for real-time soft sensor systems. It includes single-point and multiple-point touching detection, 3D deformation reconstruction, and detection of deformation in darkness.

6.2 3D Deformation Capture

To evaluate the capability of real-time deformation capture, we developed a system capable of analyzing sensor signals and performing 3D reconstruction without the need for vision equipment. The system, depicted in Figure 11, displays the reconstructed surface and updates it in real-time as a wooden stick is pressed against the sensor, demonstrating its ability to capture deformation. To visualize the deformation, two virtual planes with different subdivision parameters were selected. It should be noted that due to size limitations, the vertical displacement is more pronounced than the horizontal displacement when deformation occurs. The variation in the vertical direction of the markers corresponds to the variation in the sensor's capacitance, as shown in Figure 10. The system prototype has a delay of approximately 1 second in synchronizing the deformation. The slower reading speed of raw data during sensor deformation compared to the invariant state, as well as the use of a moving average calculation within a short time span, can both contribute to slower response times in the prototype. Nevertheless, in most real-world cases, the prototype remains capable of accurately and efficiently detecting and reflecting deformation.

To measure the accuracy of the 3D reconstruction, we used a test data set due to the complexity of visually determining the position of the reconstructed plane. Our trained model demonstrated its ability to predict the 3D geographic location of each marker with an average loss of 4e-5, compared to 3e-5 for a random sample of test data. However, it is important to exercise caution when fine-tuning the model parameters, as 3D location training is prone to overfitting. In our generalization test, we observed that pressing on the edges resulted in significantly less deformation compared to pressing in the center. This is because the edges of the sensor prototype were supported by a rigid frame, which reduced the deformation of the data. Despite the presence of occlusion or absence of light, as demonstrated in Figure 11, the prototype system was able to perform real-time reconstruction of surface deformation.

During the data collection and task evaluation phase of our prototype, we made a deliberate decision to use standard calibration weights and wooden sticks instead of participants' fingers. This decision was motivated by three primary factors. Firstly, we encountered difficulties obtaining accurate force measurements using human hands, compared to calibration weights. In order to ensure a clean and precise dataset by eliminating extraneous noise from the calibration dataset, we aimed to minimize manual work. Furthermore, we observed that using human hands resulted in less significant deformation of the sensor compared to wooden sticks. Consequently, we selected tasks that could easily verify the prototype's performance. In addition, collecting 3D deformation data using human hands posed a challenge as they frequently obscured the reflective markers, requiring a restart of the data collection

session as the camera system lost track of them. Conversely, using wooden sticks of a fixed size made it more convenient to measure and localize the touching area.

Currently, the sensor's use case is limited to pressing and touching due to the prototype's size and the number of electrodes. Therefore, our task evaluation primarily focuses on single point and multi-point touching. In future work, we plan to increase the sensor's size and electrode numbers, which would require data collection from more participants and involve more interaction types.

7 CONCLUSION AND FUTURE WORK

The present study introduces a novel low-cost soft sensor that meets the crucial criteria of being inexpensive to fabricate, easy to install, and effective. We achieve these objectives through several contributions, including the sensor layout design, material selection, automation of the manufacturing process using laser cutters and 3D printers and the development of an Arduino-based prototype solution. The accuracy of the new soft sensor was validated using a live interactive system , and experiments with different scenarios showed the generalizability of the data-driven model.

For future research, we aim to expand the use of our soft sensor by detecting the surface deformation of 3D objects with standardized mesh layout. This presents new challenges, such as mapping 2D deformation to 3D objects. To tackle this, we plan to improve the electrode arrangement by using a triangular structure, which is more resistant to deformation than a grid structure. Furthermore, we aim to increase the sensor size and number of electrodes by modernizing the fabrication process, enabling the detection of large surface deformations of objects. To handle the vast amount of raw data generated by the triangular layout, we aim to develop appropriate data-driven models. These research objectives will significantly broaden the scope of applications for our sensors, such as industrial deformation detection and the skin of robotic arms.

Another promising future direction for our soft sensor technology is in the realm of object detection. During our experimentation, we observed slight differences in the sensor signals when touched with different materials. Building on this observation, we envision a future where we can measure the electrical fields of different materials and correlate them with the sensor signals. This would enable us to accurately identify the object being touched by our soft sensor.

REFERENCES

[1] Jason Alexander, Anne Roudaut, Jürgen Steimle, Kasper Hornbæk, Miguel Bruns Alonso, Sean Follmer, and Timothy Merritt. 2018. Grand Challenges in Shape-Changing Interface Research. In *Proceedings of the 2018 CHI Conference on Human Factors in Computing Systems* (Montreal QC, Canada) *(CHI '18)*. Association for Computing Machinery, New York, NY, USA, 1–14. https://doi.org/10.1145/3173574.3173873

[2] Oluwaseun Araromi, Samuel Rosset, and Herbert Shea. 2015. High-Resolution, Large-Area Fabrication of Compliant Electrodes via Laser Ablation for Robust, Stretchable Dielectric Elastomer Actuators and Sensors. *ACS applied materials & interfaces* 7 (07 2015). https://doi.org/10.1021/acsami.5b04975

[3] Moritz Bächer, Benjamin Hepp, Fabrizio Pece, Paul G. Kry, Bernd Bickel, Bernhard Thomaszewski, and Otmar Hilliges. 2016. DefSense: Computational Design of Customized Deformable Input Devices. In *Proceedings of the 2016 CHI Conference on Human Factors in Computing Systems* (San Jose, California, USA) *(CHI '16)*. Association for Computing Machinery, New York, NY, USA, 3806–3816. https://doi.org/10.1145/2858036.2858354

[4] Rebecca Baldwin, Stan Bobovych, Ryan Robucci, Chintan Patel, and Nilanjan Banerjee. 2015. Gait Analysis for Fall Prediction Using Hierarchical Textile-Based Capacitive Sensor Arrays. In *Proceedings of the 2015 Design, Automation Test in Europe Conference Exhibition* (Grenoble, France) *(DATE '15)*. EDA Consortium, San Jose, CA, USA, 1293–1298. https://doi.org/10.7873/DATE.2015.0943

[5] Alberto Boem. 2014. Sculpton: A malleable tangible interface for sound sculpting. In *Proceedings of the 2014 Joint International Computer Music Conference and Sound and Music Computing, ICMA 2014, San Francisco, USA, 2014*. Michigan Publishing. https://doi.org/10.5281/zenodo.850671

[6] Alberto Boem and Giovanni Maria Troiano. 2019. Non-Rigid HCI: A Review of Deformable Interfaces and Input. In *Proceedings of the 2019 on Designing Interactive Systems Conference* (San Diego, CA, USA) *(DIS '19)*. Association for Computing Machinery, New York, NY, USA, 885–906. https://doi.org/10.1145/3322276.3322347

[7] R. Chatterjee and F. Matsuno. 2008. Capacitive touch sensor based user-interface : Generic design considerations and development of an wearable input device. In *2008 SICE Annual Conference*. 2299–2303. https://doi.org/10.1109/SICE.2008.4655048

[8] Eshwar Reddy Cholleti, Jonathan Stringer, Mahtab Assadian, Virginie Battmann, Chris Bowen, and Kean Aw. 2019. Highly Stretchable Capacitive Sensor with Printed Carbon Black Electrodes on Barium Titanate Elastomer Composite. *Sensors* 19, 1 (2019). https://doi.org/10.3390/s19010042

[9] Gabe Cohn, Sidhant Gupta, Tien-Jui Lee, Dan Morris, Joshua R. Smith, Matthew S. Reynolds, Desney S. Tan, and Shwetak N. Patel. 2012. An Ultra-Low-Power Human Body Motion Sensor Using Static Electric Field Sensing. In *Proceedings of the 2012 ACM Conference on Ubiquitous Computing* (Pittsburgh, Pennsylvania) *(UbiComp '12)*. Association for Computing Machinery, New York, NY, USA, 99–102. https://doi.org/10.1145/2370216.2370233

[10] Gabe Cohn, Daniel Morris, Shwetak Patel, and Desney Tan. 2012. Humantenna: Using the Body as an Antenna for Real-Time Whole-Body Interaction. In *Proceedings of the SIGCHI Conference on Human Factors in Computing Systems* (Austin, Texas, USA) *(CHI '12)*. Association for Computing Machinery, New York, NY, USA, 1901–1910. https://doi.org/10.1145/2207676.2208330

[11] Elkem. [n. d.]. *Elkem Medical Grade RTV Silicone*. https://www.elkem.com/silicones/offer/healthcare/medical-grade/room-temperature-vulcanizing/

[12] Oliver Glauser, Daniele Panozzo, Otmar Hilliges, and Olga Sorkine-Hornung. 2019. Deformation Capture via Soft and Stretchable Sensor Arrays. *ACM Trans. Graph.* 38, 2, Article 16 (mar 2019), 16 pages. https://doi.org/10.1145/3311972

[13] Oliver Glauser, Shihao Wu, Daniele Panozzo, Otmar Hilliges, and Olga Sorkine-Hornung. 2019. Interactive Hand Pose Estimation Using a Stretch-Sensing Soft Glove. *ACM Trans. Graph.* 38, 4, Article 41 (jul 2019), 15 pages. https://doi.org/10.1145/3306346.3322957

[14] Nan-Wei Gong, Jürgen Steimle, Simon Olberding, Steve Hodges, Nicholas Edward Gillian, Yoshihiro Kawahara, and Joseph A. Paradiso. 2014. PrintSense: A Versatile Sensing Technique to Support Multimodal Flexible Surface Interaction. In *Proceedings of the SIGCHI Conference on Human Factors in Computing Systems* (Toronto, Ontario, Canada) *(CHI '14)*. Association for Computing Machinery, New York, NY, USA, 1407–1410. https://doi.org/10.1145/2556288.2557173

[15] Tobias Grosse-Puppendahl, Yannick Berghoefer, Andreas Braun, Raphael Wimmer, and Arjan Kuijper. 2013. OpenCapSense: A rapid prototyping toolkit for pervasive interaction using capacitive sensing. In *2013 IEEE International Conference on Pervasive Computing and Communications (PerCom)*. 152–159. https://doi.org/10.1109/PerCom.2013.6526726

[16] Tobias Grosse-Puppendahl, Christian Holz, Gabe Cohn, Raphael Wimmer, Oskar Bechtold, Steve Hodges, Matthew S. Reynolds, and Joshua R. Smith. 2017. Finding Common Ground: A Survey of Capacitive Sensing in Human-Computer Interaction. In *Proceedings of the 2017 CHI Conference on Human Factors in Computing Systems* (Denver, Colorado, USA) *(CHI '17)*. Association for Computing Machinery, New York, NY, USA, 3293–3315. https://doi.org/10.1145/3025453.3025808

[17] Jaehyun Han, Jiseong Gu, and Geehyuk Lee. 2014. Trampoline: A Double-Sided Elastic Touch Device for Creating Reliefs. In *Proceedings of the 27th Annual ACM Symposium on User Interface Software and Technology* (Honolulu, Hawaii, USA) *(UIST '14)*. Association for Computing Machinery, New York, NY, USA, 383–388. https://doi.org/10.1145/2642918.2647381

[18] Ken Hinckley and Mike Sinclair. 1999. Touch-Sensing Input Devices. In *Proceedings of the SIGCHI Conference on Human Factors in Computing Systems* (Pittsburgh, Pennsylvania, USA) *(CHI '99)*. Association for Computing Machinery, New York, NY, USA, 223–230. https://doi.org/10.1145/302979.303045

[19] Bo Huang, Mingyu Li, Tao Mei, David McCoul, Shihao Qin, Zhanfeng Zhao, and Jianwen Zhao. 2017. Wearable Stretch Sensors for Motion Measurement of the Wrist Joint Based on Dielectric Elastomers. *Sensors* 17, 12 (2017). https://doi.org/10.3390/s17122708

[20] Joseph A Paradiso Irmandy Wicaksono. 2017. FabricKeyboard: Multimodal Textile Sensate Media as an Expressive and Deformable Musical Interface. In *NIME'17*. Aalborg University Copenhagen, 348–353. https://www.nime.org/proceedings/2017/nime2017_paper0066.pdf

[21] Heijun Jeong and Sungjoon Lim. 2016. A Stretchable Radio-Frequency Strain Sensor Using Screen Printing Technology. *Sensors* 16, 11 (2016). https://doi.org/10.3390/s16111839

[22] Hsin-Liu (Cindy) Kao, Christian Holz, Asta Roseway, Andres Calvo, and Chris Schmandt. 2016. DuoSkin: Rapidly Prototyping on-Skin User Interfaces Using Skin-Friendly Materials. In *Proceedings of the 2016 ACM International Symposium on Wearable Computers* (Heidelberg, Germany) *(ISWC '16)*. Association for Computing Machinery, New York, NY, USA, 16–23. https://doi.org/10.1145/2971763.2971777

[23] Gierad Laput, Chouchang Yang, Robert Xiao, Alanson Sample, and Chris Harrison. 2015. EM-Sense: Touch Recognition of Uninstrumented, Electrical and Electromechanical Objects. In *Proceedings of the 28th Annual ACM Symposium on User Interface Software & Technology* (Charlotte, NC, USA) *(UIST '15)*. Association for Computing Machinery, New York, NY, USA, 157–166. https://doi.org/10.1145/2807442.2807481

[24] Chris Larson, Josef Spjut, Ross Knepper, and Robert Shepherd. 2019. A Deformable Interface for Human Touch Recognition Using Stretchable Carbon Nanotube Dielectric Elastomer Sensors and Deep Neural Networks. *Soft Robotics* 6, 5 (2019), 611–620. https://doi.org/10.1089/soro.2018.0086 arXiv:https://doi.org/10.1089/soro.2018.0086 PMID: 31381482.

[25] Mathieu Le Goc, Stuart Taylor, Shahram Izadi, and Cem Keskin. 2014. A Low-Cost Transparent Electric Field Sensor for 3d Interaction on Mobile Devices. In *Proceedings of the SIGCHI Conference on Human Factors in Computing Systems* (Toronto, Ontario, Canada) *(CHI '14)*. Association for Computing Machinery, New York, NY, USA, 3167–3170. https://doi.org/10.1145/2556288.2557331

[26] Roman Lissermann, Jochen Huber, Aristotelis Hadjakos, Suranga Nanayakkara, and Max Mühlhäuser. 2014. EarPut: Augmenting Ear-Worn Devices for Ear-Based Interaction. In *Proceedings of the 26th Australian Computer-Human Interaction Conference on Designing Futures: The Future of Design* (Sydney, New South Wales, Australia) *(OzCHI '14)*. Association for Computing Machinery, New York, NY, USA, 300–307. https://doi.org/10.1145/2686612.2686655

[27] Xingxing Ma, Jiajie Guo, Kok-Meng Lee, Luye Yang, and Minghui Chen. 2019. A Soft Capacitive Wearable Sensing System for Lower-Limb Motion Monitoring. In *Intelligent Robotics and Applications: 12th International Conference, ICIRA 2019, Shenyang, China, August 8–11, 2019, Proceedings, Part IV* (Shenyang, China). Springer-Verlag, Berlin, Heidelberg, 467–479. https://doi.org/10.1007/978-3-030-27538-9_40

[28] Brian Mayton, Louis LeGrand, and Joshua R. Smith. 2010. An Electric Field Pretouch system for grasping and co-manipulation. In *2010 IEEE International Conference on Robotics and Automation*. 831–838. https://doi.org/10.1109/ROBOT.2010.5509658

[29] Andreas Mehmann, Matija Varga, Karl Gönner, and Gerhard Tröster. 2015. A Ball-Grid-Array-like Electronics-to-Textile Pocket Connector for Wearable Electronics. In *Proceedings of the 2015 ACM International Symposium on Wearable Computers* (Osaka, Japan) *(ISWC '15)*. Association for Computing Machinery, New York, NY, USA, 57–60. https://doi.org/10.1145/2802083.2802093

[30] Mohammad Faizuddin Mohd Noor, Andrew Ramsay, Stephen Hughes, Simon Rogers, John Williamson, and Roderick Murray-Smith. 2014. 28 Frames Later: Predicting Screen Touches from Back-of-Device Grip Changes. In *Proceedings of the SIGCHI Conference on Human Factors in Computing Systems* (Toronto, Ontario, Canada) *(CHI '14)*. Association for Computing Machinery, New York, NY, USA, 2005–2008. https://doi.org/10.1145/2556288.2557148

[31] T Murakami and N Nakajima. 2000. DO-IT: deformable object as input tool for 3-D geometric operation. *Computer-Aided Design* 32, 1 (2000), 5–16. https://doi.org/10.1016/S0010-4485(99)00078-0

[32] Ken Nakagaki, Luke Vink, Jared Counts, Daniel Windham, Daniel Leithinger, Sean Follmer, and Hiroshi Ishii. 2016. Materiable: Rendering Dynamic Material Properties in Response to Direct Physical Touch with Shape Changing Interfaces. In *Proceedings of the 2016 CHI Conference on Human Factors in Computing Systems* (San Jose, California, USA) *(CHI '16)*. Association for Computing Machinery, New York, NY, USA, 2764–2772. https://doi.org/10.1145/2858036.2858104

[33] Vinh P. Nguyen, Sang Ho Yoon, Ansh Verma, and Karthik Ramani. 2014. BendID: Flexible Interface for Localized Deformation Recognition. In *Proceedings of the 2014 ACM International Joint Conference on Pervasive and Ubiquitous Computing* (Seattle, Washington) *(UbiComp '14)*. Association for Computing Machinery, New York, NY, USA, 553–557. https://doi.org/10.1145/2632048.2636092

[34] Jaime Oliver and Mathew Jenkins. 2008. The Silent Drum controller: a New percussive gestural Interface. In *Proceedings of the 2008 International Computer Music Conference, ICMC 2008, Belfast, Ireland, August 24-29, 2008*. Michigan Publishing. https://hdl.handle.net/2027/spo.bbp2372.2008.118

[35] OptiTrack. [n. d.]. *OptiTrack - Motion Capture Systems*. https://optitrack.com/

[36] Patrick Parzer, Kathrin Probst, Teo Babic, Christian Rendl, Anita Vogl, Alex Olwal, and Michael Haller. 2016. FlexTiles: A Flexible, Stretchable, Formable, Pressure-Sensitive, Tactile Input Sensor. In *Proceedings of the 2016 CHI Conference Extended Abstracts on Human Factors in Computing Systems* (San Jose, California, USA) *(CHI EA '16)*. Association for Computing Machinery, New York, NY, USA, 3754–3757. https://doi.org/10.1145/2851581.2890253

[37] Patrick Parzer, Adwait Sharma, Anita Vogl, Jürgen Steimle, Alex Olwal, and Michael Haller. 2017. SmartSleeve: Real-Time Sensing of Surface and Deformation Gestures on Flexible, Interactive Textiles, Using a Hybrid Gesture Detection Pipeline. In *Proceedings of the 30th Annual ACM Symposium on User Interface Software and Technology* (Québec City, QC, Canada) *(UIST '17)*. Association for Computing Machinery, New York, NY, USA, 565–577. https://doi.org/10.1145/3126594.3126652

[38] Huaishu Peng, Jennifer Mankoff, Scott E. Hudson, and James McCann. 2015. A Layered Fabric 3D Printer for Soft Interactive Objects. In *Proceedings of the 33rd Annual ACM Conference on Human Factors in Computing Systems* (Seoul, Republic of Korea) *(CHI '15)*. Association for Computing Machinery, New York, NY, USA, 1789–1798. https://doi.org/10.1145/2702123.2702327

[39] Majken K. Rasmussen, Esben W. Pedersen, Marianne G. Petersen, and Kasper Hornbæk. 2012. Shape-Changing Interfaces: A Review of the Design Space and Open Research Questions. In *Proceedings of the SIGCHI Conference on Human Factors in Computing Systems* (Austin, Texas, USA) *(CHI '12)*. Association for Computing Machinery, New York, NY, USA, 735–744. https://doi.org/10.1145/2207676.2207781

[40] Jun Rekimoto. 2002. SmartSkin: An Infrastructure for Freehand Manipulation on Interactive Surfaces. In *Proceedings of the SIGCHI Conference on Human Factors in Computing Systems* (Minneapolis, Minnesota, USA) *(CHI '02)*. Association for Computing Machinery, New York, NY, USA, 113–120. https://doi.org/10.1145/503376.503397

[41] Christian Rendl, Patrick Greindl, Michael Haller, Martin Zirkl, Barbara Stadlober, and Paul Hartmann. 2012. *PyzoFlex: Printed Piezoelectric Pressure Sensing Foil*. Association for Computing Machinery, New York, NY, USA, 509–518. https://doi.org/10.1145/2380116.2380180

[42] Christian Rendl, David Kim, Sean Fanello, Patrick Parzer, Christoph Rhemann, Jonathan Taylor, Martin Zirkl, Gregor Scheipl, Thomas Rothländer, Michael Haller, and Shahram Izadi. 2014. FlexSense: A Transparent Self-Sensing Deformable Surface. In *Proceedings of the 27th Annual ACM Symposium on User Interface Software & Technology* (Honolulu, Hawaii, USA) *(UIST '14)*. Association for Computing Machinery, New York, NY, USA, 129–138. https://doi.org/10.1145/2642918.2647405

[43] Samuel Rosset, Oluwaseun A Araromi, Samuel Schlatter, and Herbert R Shea. 2016. Fabrication process of silicone-based dielectric elastomer actuators. *J. Vis. Exp.* 108 (feb 2016), e53423. https://doi.org/10.3791/53423

[44] Silvia Rus, Tobias Grosse-Puppendahl, and Arjan Kuijper. 2014. Recognition of bed postures using mutual capacitance sensing. In *Ambient Intelligence*. Springer, 51–66. https://doi.org/10.1007/978-3-319-14112-1_5

[45] Silvia Rus, Tobias Grosse-Puppendahl, and Arjan Kuijper. 2017. Evaluating the Recognition of Bed Postures Using Mutual Capacitance Sensing. *J. Ambient Intell. Smart Environ.* 9, 1 (jan 2017), 113–127. https://doi.org/10.3233/AIS-160414

[46] Mirza Saquib Sarwar, Yuta Dobashi, Claire Preston, Justin K. M. Wyss, Shahriar Mirabbasi, and John David Wyndham Madden. 2017. Bend, stretch, and touch: Locating a finger on an actively deformed transparent sensor array. *Science Advances* 3, 3 (2017), e1602200. https://doi.org/10.1126/sciadv.1602200 arXiv:https://www.science.org/doi/pdf/10.1126/sciadv.1602200

[47] Valkyrie Savage, Xiaohan Zhang, and Björn Hartmann. 2012. *Midas: Fabricating Custom Capacitive Touch Sensors to Prototype Interactive Objects*. Association for Computing Machinery, New York, NY, USA, 579–588. https://doi.org/10.1145/2380116.2380189

[48] Martin Schmitz, Mohammadreza Khalilbeigi, Matthias Balwierz, Roman Lissermann, Max Mühlhäuser, and Jürgen Steimle. 2015. Capricate: A Fabrication Pipeline to Design and 3D Print Capacitive Touch Sensors for Interactive Objects. In *Proceedings of the 28th Annual ACM Symposium on User Interface Software & Technology* (Charlotte, NC, USA) *(UIST '15)*. Association for Computing Machinery, New York, NY, USA, 253–258. https://doi.org/10.1145/2807442.2807503

[49] Tsuyoshi Sekitani, Hiroyoshi Nakajima, Hiroki Maeda, Takanori Fukushima, Takuzo Aida, Kenji Hata, and Takao Someya. 2009. Stretchable active-matrix organic light-emitting diode display using printable elastic conductors. *Nature materials* 8, 6 (2009), 494–499. https://doi.org/10.1038/nmat2459

[50] Gurashish Singh, Alexander Nelson, Ryan Robucci, Chintan Patel, and Nilanjan Banerjee. 2015. Inviz: Low-power personalized gesture recognition using wearable textile capacitive sensor arrays. In *2015 IEEE International Conference on Pervasive Computing and Communications (PerCom)*. 198–206. https://doi.org/10.1109/PERCOM.2015.7146529

[51] Jürgen Steimle, Andreas Jordt, and Pattie Maes. 2013. Flexpad: Highly Flexible Bending Interactions for Projected Handheld Displays. In *Proceedings of the SIGCHI Conference on Human Factors in Computing Systems* (Paris, France) *(CHI '13)*. Association for Computing Machinery, New York, NY, USA, 237–246. https://doi.org/10.1145/2470654.2470688

[52] Stratasys. [n. d.]. *Industrial 3D Printing & Additive Manufacturing - Stratasys*. https://www.stratasys.com/en/

[53] Yuta Sugiura, Masahiko Inami, and Takeo Igarashi. 2012. *A Thin Stretchable Interface for Tangential Force Measurement*. Association for Computing Machinery, New York, NY, USA, 529–536. https://doi.org/10.1145/2380116.2380182

[54] Koray Tahiroğlu, Thomas Svedström, Valtteri Wikström, Simon Overstall, Johan Kildal, and Teemu Ahmaniemi. 2014. SoundFLEX: Designing Audio to Guide Interactions with Shape-Retaining Deformable Interfaces. In *Proceedings of the 16th International Conference on Multimodal Interaction* (Istanbul, Turkey) *(ICMI '14)*. Association for Computing Machinery, New York, NY, USA, 267–274. https:

//doi.org/10.1145/2663204.2663278

[55] Giovanni Maria Troiano, Esben Warming Pedersen, and Kasper Hornbæk. 2015. Deformable Interfaces for Performing Music. In *Proceedings of the 33rd Annual ACM Conference on Human Factors in Computing Systems* (Seoul, Republic of Korea) *(CHI '15)*. Association for Computing Machinery, New York, NY, USA, 377–386. https://doi.org/10.1145/2702123.2702492

[56] Tubal. [n. d.]. *TUBALL MATRIX 601*. https://tuball.com/additives/601

[57] Tomas Unander, Hans-Erik Nilsson, and Bengt Oelmann. 2007. Printed touch sensor for interactive packaging and display. In *Polytronic 2007 - 6th International Conference on Polymers and Adhesives in Microelectronics and Photonics*. 12–17. https://doi.org/10.1109/POLYTR.2007.4339128

[58] Katia Vega, Marcio Cunha, and Hugo Fuks. 2015. Hairware: The Conscious Use of Unconscious Auto-Contact Behaviors. In *Proceedings of the 20th International Conference on Intelligent User Interfaces* (Atlanta, Georgia, USA) *(IUI '15)*. Association for Computing Machinery, New York, NY, USA, 78–86. https://doi.org/10.1145/2678025.2701404

[59] Martin Weigel, Tong Lu, Gilles Bailly, Antti Oulasvirta, Carmel Majidi, and Jürgen Steimle. 2015. ISkin: Flexible, Stretchable and Visually Customizable On-Body Touch Sensors for Mobile Computing. In *Proceedings of the 33rd Annual ACM Conference on Human Factors in Computing Systems* (Seoul, Republic of Korea) *(CHI '15)*. Association for Computing Machinery, New York, NY, USA, 2991–3000. https://doi.org/10.1145/2702123.2702391

[60] Michael Wessely, Theophanis Tsandilas, and Wendy E. Mackay. 2016. Stretchis: Fabricating Highly Stretchable User Interfaces. In *Proceedings of the 29th Annual Symposium on User Interface Software and Technology* (Tokyo, Japan) *(UIST '16)*. Association for Computing Machinery, New York, NY, USA, 697–704. https://doi.org/10.1145/2984511.2984521

[61] Valtteri Wikström, Simon Overstall, Koray Tahiroğlu, Johan Kildal, and Teemu Ahmaniemi. 2013. MARSUI: Malleable Audio-Reactive Shape-Retaining User Interface. In *CHI '13 Extended Abstracts on Human Factors in Computing Systems* (Paris, France) *(CHI EA '13)*. Association for Computing Machinery, New York, NY, USA, 3151–3154. https://doi.org/10.1145/2468356.2479633

[62] Raphael Wimmer, Matthias Kranz, Sebastian Boring, and Albrecht Schmidt. 2007. A Capacitive Sensing Toolkit for Pervasive Activity Detection and Recognition. In *Fifth Annual IEEE International Conference on Pervasive Computing and Communications (PerCom'07)*. 171–180. https://doi.org/10.1109/PERCOM.2007.1

[63] Jin Yan, Austin Downey, Alessandro Cancelli, Simon Laflamme, An Chen, Jian Li, and Filippo Ubertini. 2019. Concrete Crack Detection and Monitoring Using a Capacitive Dense Sensor Array. *Sensors* 19, 8 (2019). https://doi.org/10.3390/s19081843

[64] Doruk Yildirim, Luis Edgardo Fraguada, and Elizabeth Esther Bigger. 2019. DualSkin: Ambient Electric Field Sensing Wearable. In *Proceedings of the 23rd International Symposium on Wearable Computers* (London, United Kingdom) *(ISWC '19)*. Association for Computing Machinery, New York, NY, USA, 339–345. https://doi.org/10.1145/3341163.3346931

[65] Sang Ho Yoon, Ke Huo, Yunbo Zhang, Guiming Chen, Luis Paredes, Subramanian Chidambaram, and Karthik Ramani. 2017. ISoft: A Customizable Soft Sensor with Real-Time Continuous Contact and Stretching Sensing. In *Proceedings of the 30th Annual ACM Symposium on User Interface Software and Technology* (Québec City, QC, Canada) *(UIST '17)*. Association for Computing Machinery, New York, NY, USA, 665–678. https://doi.org/10.1145/3126594.3126654

[66] Sang Ho Yoon, Luis Paredes, Ke Huo, and Karthik Ramani. 2018. MultiSoft: Soft Sensor Enabling Real-Time Multimodal Sensing with Contact Localization and Deformation Classification. *Proc. ACM Interact. Mob. Wearable Ubiquitous Technol.* 2, 3, Article 145 (sep 2018), 21 pages. https://doi.org/10.1145/3264955